Nanoscale Res Lett (2010) 5:454–463
DOI 10.1007/s11671-010-9543-z

SPECIAL ISSUE ARTICLE

Nanofabrication with Pulsed Lasers

A. V. Kabashin · Ph. Delaporte · A. Pereira · D. Grojo · R. Torres · Th. Sarnet · M. Sentis

Received: 17 November 2009 / Accepted: 16 January 2010 / Published online: 24 February 2010

Abstract An overview of pulsed laser-assisted methods for nanofabrication, which are currently developed in our Institute (LP3), is presented. The methods compass a variety of possibilities for material nanostructuring offered by laser–matter interactions and imply either the nanostructuring of the laser-illuminated surface itself, as in cases of direct laser ablation or laser plasma-assisted treatment of semiconductors to form light-absorbing and light-emitting nano-architectures, as well as periodic nanoarrays, or laser-assisted production of nanoclusters and their controlled growth in gaseous or liquid medium to form nanostructured films or colloidal nanoparticles. Nanomaterials synthesized by laser-assisted methods have a variety of unique properties, not reproducible by any other route, and are of importance for photovoltaics, optoelectronics, biological sensing, imaging and therapeutics.

Keywords Laser nanofabrication · Laser ablation · Semiconductor and plasmonic nanostructures · Colloidal nanoparticles

A. V. Kabashin (✉) · Ph. Delaporte · A. Pereira · D. Grojo · R. Torres · Th. Sarnet · M. Sentis
Lasers, Plasmas et Procédés Photoniques (LP3, UMR 6182 CNRS), Université de la Méditerranée, Campus de Luminy-case 917, 13288 Marseille Cedex 9, France
e-mail: kabashin@lp3.univ-mrs.fr

Present Address:
A. Pereira
Laboratoire de Physico-Chimie des Matériaux Luminescents, LPCML (UMR 5620 CNRS), Domaine Scientifique de la Doua, Université Claude Bernard Lyon 1, 10 rue Ada Byron, 69622 Villeurbanne, France

Introduction

When nanostructured, many materials start to exhibit new optical properties making them unique for a plethora of applications. In particular, despite small and indirect band gaps in the bulk state, the nanostructured IV group semiconductors (e.g. Si, Ge) become efficient size-dependent emitters in the visible light range [1, 2], but also can work as photosensitizers to generate singlet oxygen under photoexcitation [3, 4]. Another prominent example relates to noble metal nanostructures, which provide a number of unique plasmonic effects, including size-dependent absorption peaks [5, 6], drastic local electric field enhancement [7, 8], resolution beyond the diffraction limit [9], nanotrapping [10] etc. These new properties of emerging nanomaterials appear to be extremely promising for photovoltaics and optoelectronics, as well as for biological sensing, imaging and therapeutics.

The employment of pulsed lasers offers a novel unique tool for nanofabrication [11]. When focused on the surface of a solid target, pulsed laser radiation causes a variety of effects, including heating, melting and finally ablation of the target and such processes can lead to an efficient material nanostructuring, as shown in Fig. 1. First, the laser-assisted removal of material from the irradiated spot can result in a spontaneous formation of variety of periodic micro- and nanoarchitectures within this spot [12–16]. Second, laser ablation of material from a solid target leads to the production of nanoclusters [17–20]. When produced in gaseous environment or in vacuum, these nanoclusters can then be deposited on a substrate yielding to the formation of a nanostructured film [17, 21–24]. When produced in liquid environment, the nanoclusters can be released into the liquid forming a colloidal nanoparticle solution [25–32]. In all cases, properties of formed

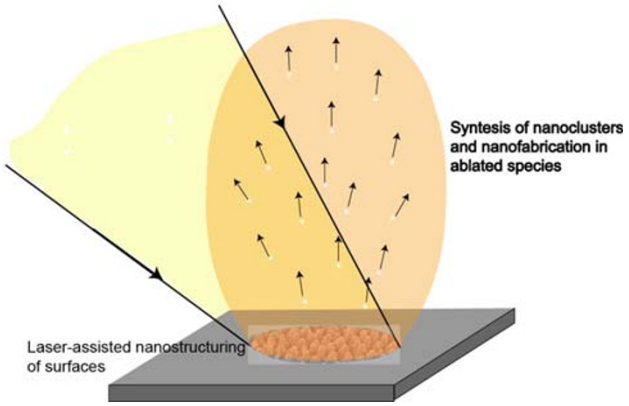

Fig. 1 Schematics of laser–target interaction and material nanostructuring

nanostructures can be unique and not reproducible by any other route [27–33]. As an example, the fabrication of nanoparticles in aqueous solutions does not require any chemical reducing agent, which conditions unique surface chemistry and purity of produced nanomaterials [28, 29]. Furthermore, when synthesized in clean, biocompatible environment, laser-synthesized nanomaterials are exempt of any residual toxicity that is typical for chemically synthesized nanoparticles [32, 33].

In this paper, we review laser-assisted technologies, developed by LP3 members, which are now available in our Institute.

Laser-assisted Nanostructuring of Surfaces

Properties of laser-materials interaction are known to be strongly dependent on parameters of laser radiation. Among these parameters, the wavelength and pulse length are especially important to determine the efficiency of radiation absorption, dynamics of plasma plume expansion and nanoclustering [11]. Ultraviolet, visible and near-infrared lasers are normally considered as most adequate for laser ablative tasks. Indeed, most industrially important materials efficiently absorb laser radiation in the spectral range of 200–1,000 nm, yielding to material ablation and nanostructuring. In addition, radiation of UV and visible lasers is relatively transparent to laser plasma, which minimizes laser beam distortions and power losses before reaching the target. In contrast, the interaction of infrared radiation (1–11 μm) with materials is characterized by a strong energy absorption by plasma itself, which completely changes conditions of nanostructuring. The pulse length is another important parameter in laser–matter interaction. Micro- and nanosecond laser–matter interactions are typically associated with long ablation regime, in which the ablation process takes place during the laser pulse itself. In contrast, pico- and femtosecond lasers offer short ablation regimes, in which moments of radiation absorption and material ablation are temporally separated. Although multi-pulse laser ablation from the target surface is always accompanied by the formation of micro- and nanoscale features and periodic structures [12–16, 34], properties of these features strongly depend on the wavelength and pulse length. Therefore, depending on the task, one can select appropriate radiation parameters to condition the ablation regime and obtain prescribed properties of laser-synthesized nanostructures. Below, we give several examples of laser-assisted methodologies to fabricate nanostructures within the irradiation spot.

Femtosecond Laser Ablation of Si: Formation of Black Si for Photovoltaics Applications

It is accepted that femtosecond pulses give at least two major advantages to micromachining compared to nanosecond and longer pulses [35, 36]: (1) the reduction of the pulse energy which is necessary to induce ablation for fixed laser wavelength and focussing conditions and (2) a significant reduction or complete removal of heat-affected zone (HAZ) and, as consequence, the improvement of the contour sharpness for the laser-processed structures. The second advantage is a direct consequence of the pulse being shorter than the heat diffusion time, given by the phonon transport. As in the case of nanosecond- and microsecond laser ablation, multi-pulse femtosecond ablation leads to a spontaneous formation of nanoarchitectures [14, 37–40]. However, in contrast to long ablation, the fs regime is characterized by the absence of target melting effects, yielding to the formation of clean micro- and nanoscale features. In particular, using multi-pulse fs ablation of Si in the presence of SF_6 reactive gas, Mazur et al. [14, 37] managed to fabricate extremely narrow micro-spikes within the irradiation spot, which are capable of efficiently absorbing light in the visible and infrared ranges. The efficient absorption of light exceeding 95% in the visible was attributed to a geometric multi-reflection effect offered by a unique spike-based structure, while the enhanced absorption in the infrared was explained by a sulphur doping [37]. Due to the wide-range absorption effect, the produced spike-based structure was called "black silicon" and was later used for the development of Si-based photodetectors. It is worth noting that such absorptive features cannot be reproduced by any alternative non-laser route. Other studies (see, e.g. [41]) reported the fabrication of nanostructured metal films exhibiting colours ("coloured metals") using similar fs ablation approach.

Our sub-project is devoted to the fabrication of "black silicon" structures for photovoltaics solar panel applications. The choice of photovoltaics as target application

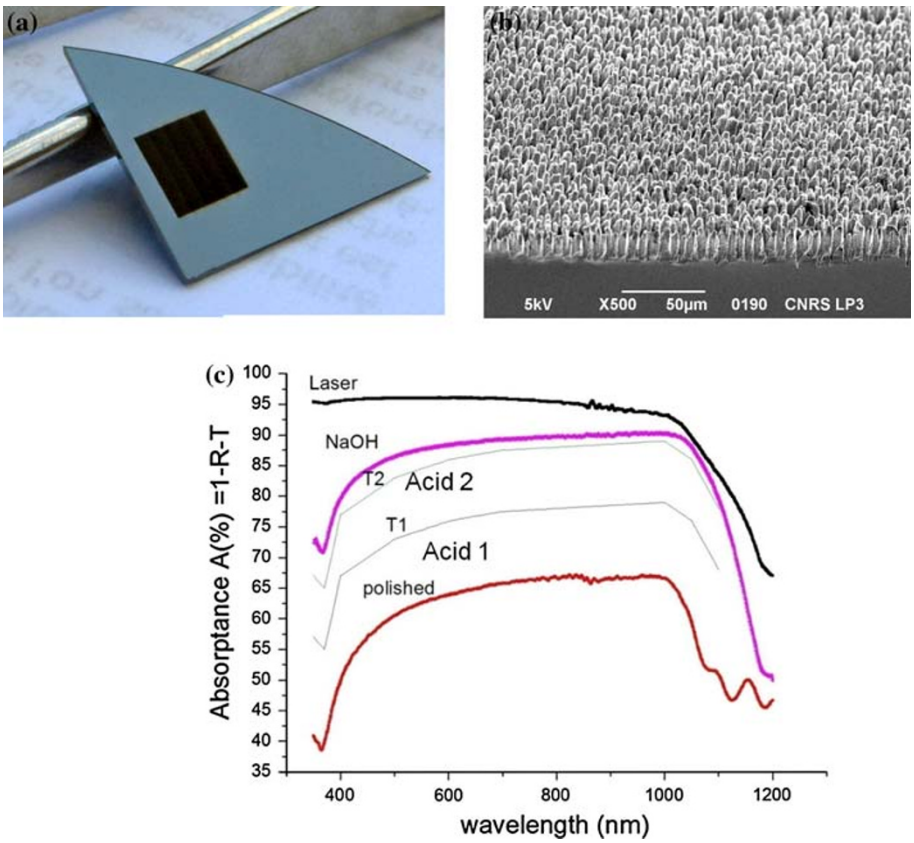

Fig. 2 **a** Typical image of "black silicon" spot fabricated on a Si wafer by multi-pulse fs laser ablation in vacuum; **b** Typical scanning electron microscopy (*SEM*) image of penguin-like structure of black silicon; **c** Typical absorption spectra from "black silicon" and silicon treated by different methods

imposes new criteria on nanostructuring conditions. First, these applications require a high absorption mostly in the visible—near-IR range (300–1,000 nm), which enables us to exclude the necessity of using sulphur-based doping species. Second, these applications require uniform high-quality doping of nanostructured layers to maximize the photovoltage response. We succeeded in developing of a novel methodology to produce "black silicon" with such parameters, employing a Ti:Sapphire laser (wavelength 800 nm, pulse energy 5 mJ, repetition rate 1 kHz) [42]. In contrast to [14, 37], we carry out multi-pulse laser processing in vacuum under the residual pressure of (1–5) $\times$ 10^{-5} mBar. In addition, we avoid the doping procedure during the laser processing process and do it afterwards. To achieve a high quality doping of deep layers, the laser-structured samples are boron implanted by Plasma immersion (PULSION, BF3, 2 kV, 900°C, 30 min) and thermally annealed (TA). The junction depth obtained by this method is estimated to be about 150 nm, which is much shallower than the 3D laser structures; therefore, the junction follows the topography of the structures. Figure 2a demonstrates a silicon wafer surface after the laser processing and boron implantation procedure. Here, a rectangular area of 3 $\times$ 2 cm^2 is written by a programmed displacement with the speed of 150 µm/s of a femtosecond laser beam having the spot size of 35 $\times$ 35 μm^2. One can clearly see a black area on the silicon wafer associated with "black silicon". As shown in Fig. 2b, the treated surface contains penguin-like nanospikes with the length of up to 10 µm and sub-µm lateral dimensions. Although the morphology of femtosecond laser-treated surface is rather different compared to narrow spike-like structures in [14, 37], it is also characterized by an enhanced absorption in the visible range exceeding 90% (Fig. 2c). Depositing grating-like contacts on the top on the treated area, we were able to obtain the amplification of photocurrent by 50% compared to the untreated surface area. Such result was attributed to an enhanced absorption granted by the penguin-like structures, much larger surface of nanostructured silicon used for signal collection, and high quality of boron implantation offered by the post-ablation plasma implantation procedure. The fabricated structures are now actively tested as photovoltaics solar cells.

Laser Plasma-assisted Nanostructuring of Surfaces

As we mentioned above, UV or ultrashort lasers contribute to a good radiation absorption by the target itself, while plasma remains relatively transparent to the incoming radiation. Such parameters ensure good quality of surface treatment in laser processing tasks. The plasma effect can be further minimized by reducing the pressure of the

ambient gas. Depending on plasma plume size conditioned by the ambient gas pressure, the material can be re-deposited either within the irradiation spot (for high atmospheric pressure) or into the environment (for reduced pressures). In particular, for atmospheric pressure, the ablation process results in the formation of a deep crater, containing microscale spikes, covered by re-deposited nanoparticles [13–16]. In this case, chemical transformations in ablated species are minimal, since the ablated material rapidly cools down while interacting with the environment [24, 43].

We recently introduced a novel method for surface nanostructuring, which is characterized by radically different nanofabrication conditions [44–49]. The method may look paradoxical, since it disaccords with main principles of laser processing requiring the minimization of plasma-related effects as one of main conditions to achieve high quality of laser treatment. In contrast, in this method, plasma-associated effects are amplified by all possible means. Basically, we use infrared radiation from CO_2 laser, which is strongly absorbed by the plasma itself. When focused in air and any other gas having atmospheric pressure, infrared radiation is capable of efficiently igniting the gas breakdown and this phenomenon is called the "laser spark". The presence of a target decreases the breakdown threshold by 2–3 orders of magnitude [50]. In the latter case, the target serves to provide first electrons. Then, an avalanche plasma discharge develops in ambient air moving towards the focusing lens. Absorbing main radiation power through the inverse Bremsstrahlung mechanism, the plasma accumulates an enormous amount of energy and is supposed to radically change conditions of nanocluster production and growth [51]. Indeed, in contrast to conventional laser ablation, the ablated species find themselves in a plasma "reactor" with extremely high temperatures (10^4 K) [52] and strong electromagnetic fields [53–56], yielding to a deep chemical transformation of properties of ablated clusters. The clusters then move back to the irradiated spot forming a film of clearly separated and densely packed spherical nanoparticles, as shown in Fig. 3a. The size of nanoparticles can vary for different materials, but is usually between 20 and 70 nm. The increase of plasma intensity can also lead to a coagulation of nanoparticles and the formation of much larger microscale spherical features. Nanostructures treated by this method have a specific texture with separated densely packed crystalline nanoparticle constituents, which contribute to unique optical properties. In particular, in the case of the laser plasma-based treatment of Zn in ambient air, the produced ZnO nanostructures exhibit very strong exciton-related peak around 380–385 nm under photoexcitation, whereas photoluminescence peaks associated with defects are essentially absent [49]. Furthermore, such nanostructure is capable of providing the mirror-less random lasing effect, arising as a result of a simultaneous strong amplification and scattering in a highly disordered medium [48]. Such effect is normally observed by the appearance of several extremely narrow lines within the exciton emission band under the increase of the pumping laser power. In the case of Si and Ge, the laser plasma treatment leads the formation of nanostructures, which are capable of generating strong photoluminescence (PL) in the visible [44–47]. Figure 3b shows PL properties of Si nanostructures fabricated by the laser plasma-based treatment. One can see two PL bands around 2.1 and 3.25 eV, associated with Si-based nanostructures. In the case of Ge, the PL bands are slightly different and situated around 2.2 and 2.9 eV [47].

Near-field Nanoparticle-assisted Nanostructuring of Surfaces: Fabrication of Patterned Nanoarrays

This sub-project addresses the formation of periodic nanoarrays by laser-assisted methodologies. The methodology implies two steps [57]: (1) laser ablation to form programmed periodic nanoscale features on a sacrificial surface layer; (2) post-ablation deposition/chemical treatment step to fabricate nanoarrays. The first step is based on the use of near-field particle-assisted ablation to produce nanoscale features on various substrates [58–61]. A monolayer of self-assembled SiO_2 spheres is formed on a 20-nm alumina (Al_2O_3) film, as shown schematically in Fig. 4a. Then, pores are optically drilled in the Al_2O_3 film

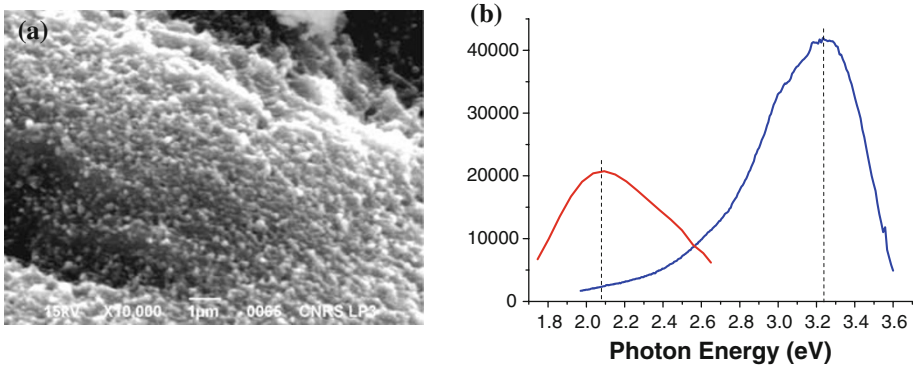

Fig. 3 **a** Typical image of Si-based nanostructures prepared by laser plasma-assisted treatment of a Si wafer; **b** Photoluminescence spectra from laser plasma-treated nanostructured Si spots for different pumping wavelengths (325 and 488 nm)

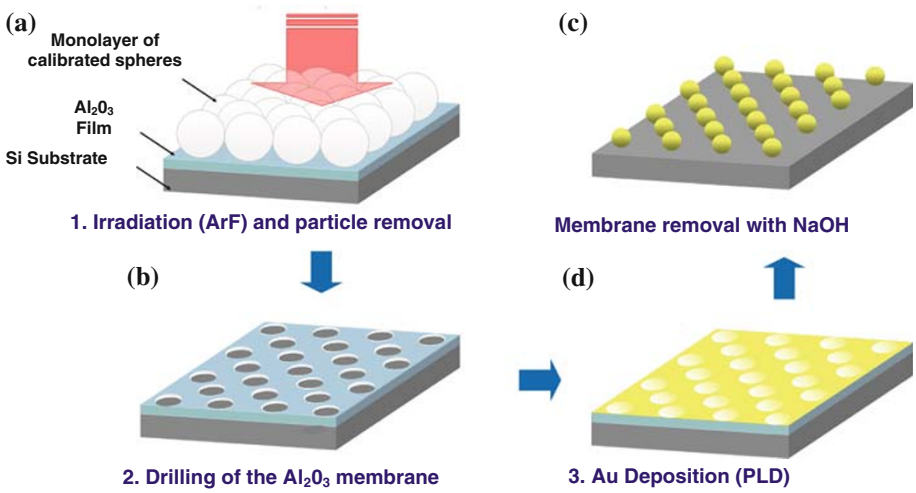

Fig. 4 Nanodot array fabrication. **a** A monolayer of spheres deposited on a thin alumina film is illuminated with a single laser pulse. **b** Near-field enhancement underneath the spheres leads to the parallel nanodrilling of the film. **c** A metal (gold in our case) is then deposited and the alumina membrane is dissolved in basic solution. **d** An ordered Au nanodot array is then obtained on the silicon substrate

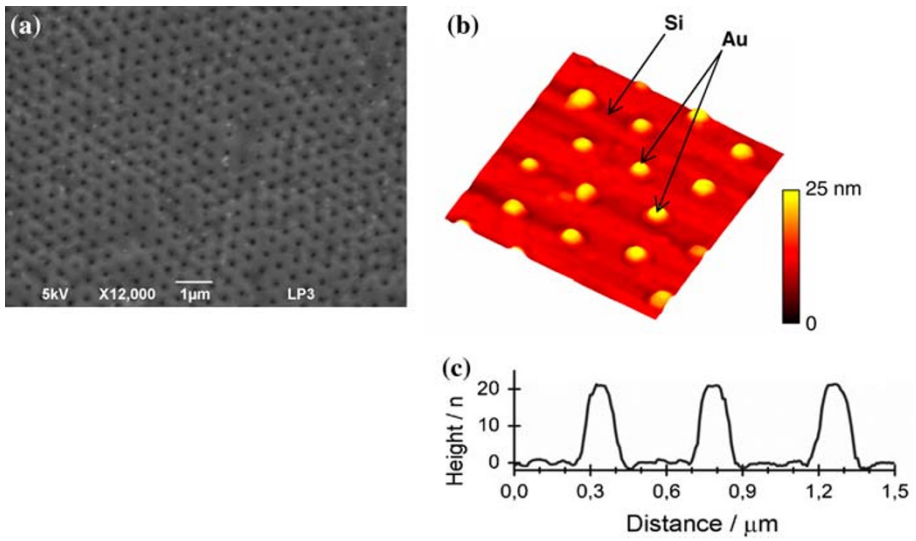

Fig. 5 **a** SEM image of an Al_2O_3 thin film (20 nm) deposited on a Si substrate and simultaneously drilled by the near-field enhancement of a single nanosecond laser pulse, which is produced by a lattice of SiO_2 spheres ($R = 250$ nm); **b** AFM image and **c** depth profile of gold nanodots created on silicon substrates by the LF-PAM-based process

by particle-assisted near-field enhancement. This is accomplished through the illumination of the spheres with a single nanosecond laser pulse at the wavelength of 193 nm. Such process leads to the local removal of the 20-nm-thick Al_2O_3 film under each sphere. Since the spheres are arranged in a hexagonal array at the surface of the substrate, the Al_2O_3 film is decorated with an ordered arrangement of holes (Fig. 4b). The second step employs the laser-fabricated porous alumina membrane (LF-PAM) as a mask for the deposition of metal (Fig. 4c). Then, the alumina layer is dissolved yielding to the production of a series of ordered metal nanodots on the surface of the substrate (Fig. 4d). One of the main advantages of the proposed method consists in a possibility of producing nanodot arrays of functional materials, independently of the nature of the substrate.

In particular, the proposed methodology can be used to fabricate an ordered array of gold nanodots (plasmonic arrays). Figure 5a shows an image of an Al_2O_3 thin film after drilling holes by 250-nm silica particle-assisted laser ablation. One can see that the laser-drilled holes are relatively uniform with the mean size of holes of about 100 nm, while the distance between the nanoholes is well conditioned by the size of self-assembled silica microparticles. As shown in Fig. 5b, c, the second deposition/chemical treatment step leads to the formation of high quality plasmonic arrays based on gold nanodots with the size of features less than 100 nm. These nanodot arrays are of importance for biosensing applications [62, 63].

Laser Ablative Synthesis of Nanoclusters

The evolution of properties of formed nanostructures after the ablation process is mainly determined by the interaction of the species with the environment. In fact, in the first approximation, the nanocluster formation process can be described by the classical theory of condensation and

nucleation in a vapour layer [64, 65]. However, the growth of nanoclusters strongly depends on initial parameters of ablated species (energy, angular distribution, density) and by laser interaction with the environment, which are conditioned by characteristics of pumping radiation. In particular, the radiation can directly affect the nucleation process if the pumping laser pulse is long enough. Indeed, the energy of photons can be sufficient to produce nucleation centres, change the dynamics of the nuclei growth and modify the diffusion of species in the vapour phase. Below, we give a review of experimental results on the laser ablative nanostructure growth.

Laser Ablation in Residual Gases and Deposition of Nanostructured Films

The first possibility is related to the ablation of material in gaseous environment and the deposition of ablated species onto a substrate in pulsed laser deposition (PLD) geometry. In this geometry, the employment of a UV radiation from an excimer laser is normally preferable [11]. UV radiation is well absorbed by most industrially important materials, while the formed plasma plume is relatively transparent to it. The material can be in general ablated in vacuum; but due to a low probability of nanocluster coalescence in vacuum, it is difficult to control their growth and the nanoclusters normally deposit as ablated, forming a dense film with a significant amorphous fraction. Therefore, it is important to have a residual neutral light gas to affect the growth procedure. In this case, nanoclusters cool down under collisions with gas molecules or atoms, which contribute to their coalescence in the vapour phase. Under such conditions, the nanocluster growth process can be efficiently controlled by varying the pressure of the ambient gas [23, 66, 67].

To fabricate Si-based nanostructured films, we normally use radiation of a pulsed ArF or KrF lasers (193 or 248 nm, respectively, 15 ns FWHM, repetition rate 30 Hz) to ablate material from a rotating Si target. The radiation is focused at the incident angle of 45° to the surface. A substrate is

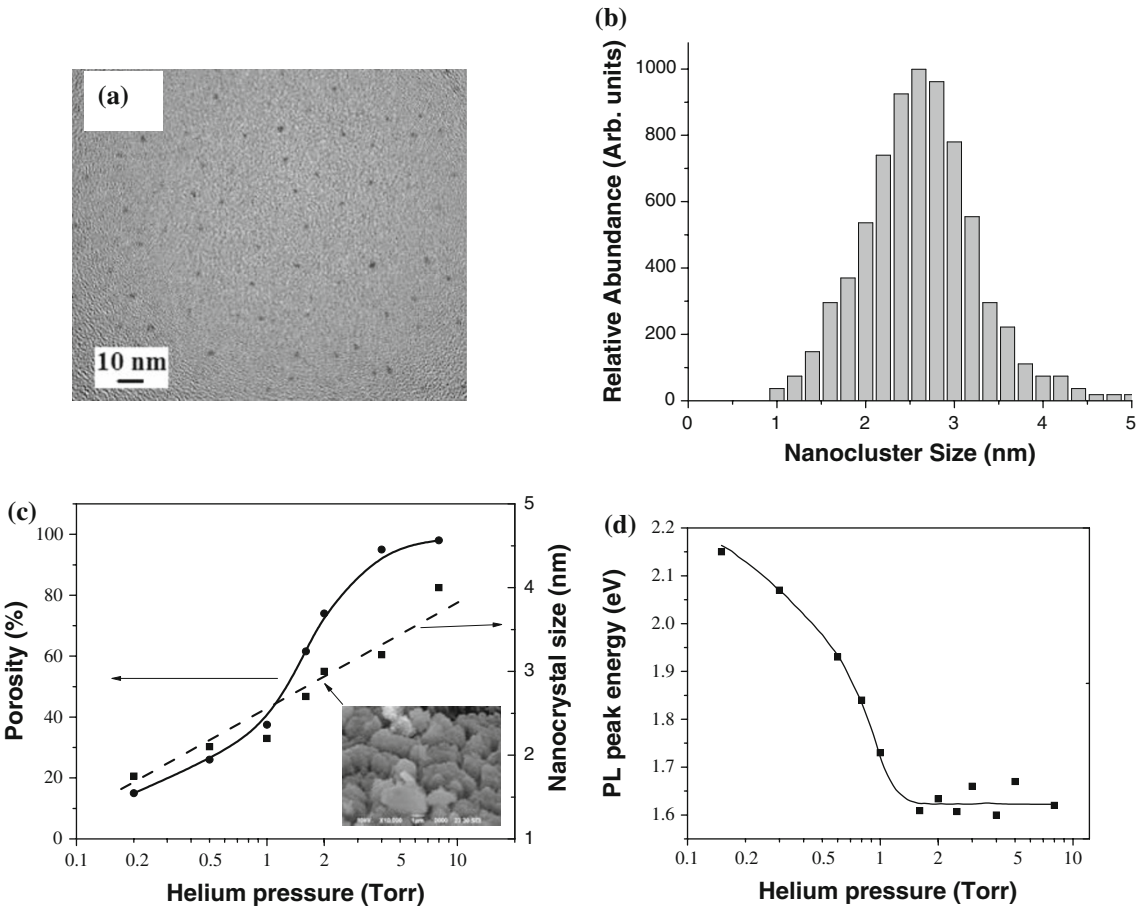

Fig. 6 Transmission electron microscopy image of Si nanoparticles fabricated by pulsed laser ablation at 2 Torr of He (**a**) and corresponding nanocluster size distribution (**b**); **c** Dependence of the nanocrystal size (*dashed line*) and film porosity (*solid line*) on the pressure of He during the deposition; *Inset* typical scanning electron microscopy image of films prepared by pulsed laser ablation; **d** Dependence of the position of PL peak from laser-ablated films on the gas pressure during the deposition

placed on a rotating holder in front of the target. The experimental chamber is filled with helium for a deposition at a constant pressure ranging between 0.05 and 10 Torr. The film thickness after several thousands laser shots is 100–700 nm.

Figure 6 shows a transmission electron microscopy (TEM) image of several isolated nanoparticles, synthesized by laser ablation from a Si target and deposited on a carbon-coated TEM grid (a) and corresponding nanoparticle size distribution (b). One can see that the produced nanoclusters are very small with the size in the range of 1–4 nm. As shown in Fig. 6c, the mean size of nanoparticles slightly increases under the increase of He pressure. For example, the increase of the pressure from 0.5 to 8 Torr results in the increase of the nanoparticle size from 1.5 to 4 nm. Another important feature relates to essentially porous texture of the films prepared by pulsed laser deposition, as illustrated by the inset of Fig. 6c, and the porosity of films increases with the increase of the ambient gas pressure (Fig. 6c). Indeed, while the deposition under 1 Torr results only in some germs of roughness, the experiment under 2 Torr provides a developed porous structure with pore size of about 50–100 nm. A further pressure increase up to 4 Torr leads to a formation of web-like aggregations of particles. As shown in Fig. 6c, the deposition of films at high pressures (>4 Torr) leads to porosities exceeding 90%, corresponding to the formation of powders on the substrate. Thus, the pressure of the ambient gas appears to be one of key parameters, which determines both the size of synthesized nanocrystals and the porosity of deposited nanostructured layers. Such a strong impact of the gas pressure on nanoclustering process suggests the importance of cooling of ablated species under their collisions with gas atoms. If the pressure of the gas is high enough, the nanoclusters experience a sufficient number of collisions to rapidly cool down and crystallize in the vapour phase. As a result, they arrive on the substrate in the form of a powder. In contrast, low collision regime at low pressures advantages the formation of dense and low-porous films.

It is important that all Si-based films prepared by the PLD method exhibit strong visible emission (PL) under photoexcitation, while PL properties of the films are quite different for films of different porosities. Low-porous films $P < 40\%$, deposited at reduced pressures $P < 1.5$ Torr, exhibit relatively weak PL with peak energy strongly depending on the gas pressure. In particular, the pressure decrease from 1.5 to 0.15 Torr in different depositions causes a blue shift of the peak from 1.6 to 2.15 eV, as shown in Fig. 6d. In contrast, films with an enhanced porosity $P > 40\%$, deposited at higher pressures, provide only spectra with fixed peaks. The first band (1.6–1.7 eV) is independent of the pressure and can be seen just after the fabrication process. An additional 2.2–2.3 eV band can appear under the oxidation of samples in humid air. Here, PL properties of low-porous films (porosity <40%) are almost unchangeable under these conditions, while the integral PL intensity from highly porous films significantly increases with the prolonged oxidation. We attribute such a difference of PL properties to the impact of post-fabrication natural oxidation, controlled by the level of porosity. Dense and self-coagulated structures of the films fabricated under $P < 1$ Torr minimize the impact of ambient atmosphere on the film properties; and for these films, mechanisms related to core silicon crystals became predominant. Since the blue shift of the spectra under the decrease of helium residual pressure is accompanied by a certain decrease of the nanocrystal size, the quantum confinement mechanism [1] can be considered as one of main opportunities. In contrast, a high porosity enhances the surface area, which is subjected to surface chemistry modifications due to interactions of nanocrystallites with oxygen. This can drastically enhance the role of oxidation in the formation of PL centres and the domination of oxygen-related PL mechanisms connected either to defects in the SiO_2 structure (usually, this mechanism provides 2–2.4 eV PL [68]) or to the interfacial layer (1.65 eV) [69].

Ultra-short Laser Ablation in Liquid Environment to Form Colloidal Nanoparticles

In the case of liquid ambience, laser ablation process leads to the release of nanoclusters into the liquid and the formation of a colloidal nanoparticle solution [11]. In contrast to conventional chemical reduction methods, this method enables avoidance of the use of toxic chemical reduction agents to control the growth of the nano-particles. As an example, the laser ablation-based synthesis can be implemented in pure deionized water. The independence of laser-based synthesis of dirty colloidal chemistry makes it unique for the fabrication of markers of bioanalytes for sensing and imaging applications. In pure water, however, or any other aqueous solution exempted of additional chemically active components, the size of nanoparticles produced tends to be relatively large, since a natural coalescence of hot ablated nanoclusters cannot be easily overcome. In particular, nanosecond laser-based ablation used in most works, generally gives relatively large (10–300 nm) and strongly dispersed (50–300 nm) particles [25–28]. Although certain size control can be achieved by decreasing the wavelength of pumping radiation or varying the laser fluence, the range of size variations stays rather moderate in the nanosecond pulse case. Mafune [27] showed that size characteristics of nanoparticles can be improved by adding some reactive surfactants such as sodium dodecyl sulphate (SDS) or CTAB during the

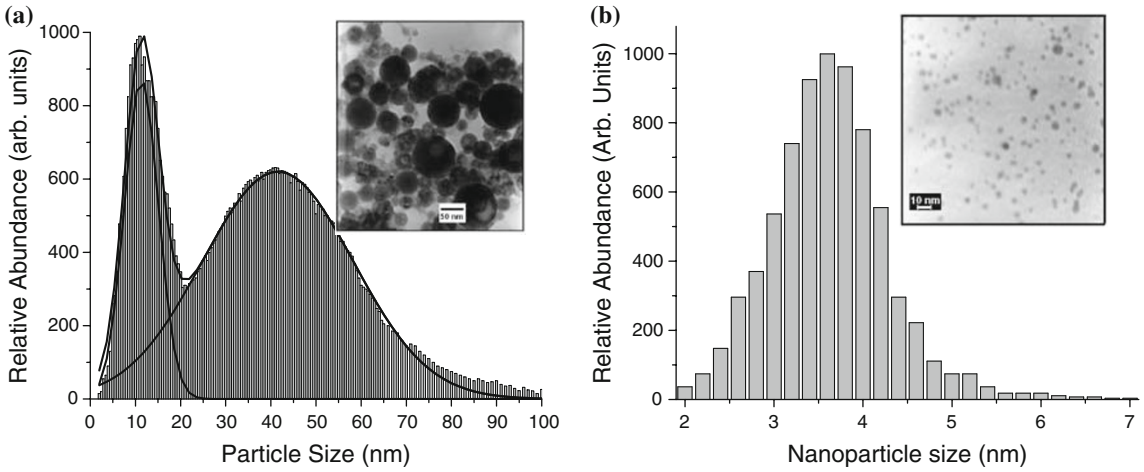

Fig. 7 Transmission electron microscopy images and corresponding size distributions of **a** TiO_x nanoparticles prepared by fs laser ablation from a Ti target in deionized water; **b** gold nanoparticles prepared in aqueous solution of polyethylene glycol

ablation. As an example, thiol-containing SDS covered gold nanoclusters just after their production and thus protected them from further coalescence. However, bioimaging applications of so produced nanoparticles are hardly possible since the surfactants are not biocompatible.

We recently proposed a femtosecond laser ablation-based method for nanoparticle synthesis, which makes possible an efficient control of size of prepared nanoparticles by varying physical parameters [28–33]. The experiments are normally carried out with an Ytterbium (400 fs FWHM, 1,025 nm, 1 kHz) or a Ti/Sapphire laser (110 fs FWHM, 800 nm, 1 μJ/pulse, 1 kHz). The radiation is focused onto a target of different materials (Au, Ag, Si, Ti, Cu), which is placed on the bottom of a glass vessel filled with aqueous solutions. The vessel is placed on a horizontal moving platform to avoid the ablation of material from the same area. The ablation experiments are carried out in pure deionized water and in aqueous solutions (biopolymers, cyclodextrins).

When performed in relatively neutral environment such as deionized water, fs laser ablation normally leads to the formation of two nanoparticle populations, independently on the material of the target, as shown in Fig. 7. The first population is characterized by a small mean nanoparticle size and narrow size dispersion, whereas the second one has a much larger mean size and broader size dispersion. The presence of the two populations suggests the involvement of two different mechanisms of nanoparticle growth. The production of the first, less dispersed population is characterized by the absence of target melting effects, suggesting direct radiation-related ablation of material [28]. In contrast, the production of the highly dispersed population is accompanied by a strong melting of material inside the ablated crater. This melting is usually attributed to the explosion of a cavitation bubble formed as a result of energy transfer from laser plasma to the liquid [11]. It is important that in the fs laser ablation regime, the nanoparticle size can be efficiently controlled by varying the intensity of radiation during the nanosynthesis process. In particular, the mean size of gold nanoparticles can be reduced from 120 to 4 nm by the decrease of laser fluence down to the threshold values [28]. Similar effect can be achieved by changing the radiation focusing on the target surface [29]. Such efficient method of size control, not possible with nanosecond or microsecond pulses, is granted by specific conditions of fs laser–materials interaction. In the fs ablation regime, much less radiation energy is transferred to the cavitation bubble (15% compared to 80% in the nanosecond pulse regime [70]). We believe that the decrease of the laser fluence down to near-threshold values enables one to completely avoid cavitation phenomena and thus eliminate the second highly size-dispersed nanoparticle population. In addition, the decrease of the laser fluence changes parameters of ablated nanoclusters (energy, angular distribution etc.), which can in turn affect the final size of nanoparticles of the first population. In particular, using this method in the case of gold, we managed to vary the size of synthesized nanoparticles between 4 and 20 nm [28].

Another important issue is related to chemical properties of laser-synthesized nanoparticles. Since the nanoparticles are produced by pure physical ablation from a target without the involvement of any specific chemicals, surface chemistry of these nanoparticles can drastically differ from that of counterparts prepared by conventional colloidal chemistry [30, 31, 71–73]. In particular, laser-synthesized gold becomes susceptible to oxidation and, in contrast to chemically prepared gold, the surface of these nanoparticles is partially covered by a layer of oxide. Furthermore, the oxidized nanoparticle surface can have different termination, depending on the pH of the environment. The

oxidized portion of the gold surface normally has Au–O– groups at pH > 5.8 and increasing numbers of Au–OH groups at pH < 5.8 [71]. This oxide-related surface termination makes possible interactions of gold nanoparticles with groups, for which conventional gold is normally inert. A prominent example of new gold chemistry is related to the use of biopolymers [72] and oligosaccharides [30]. Although these substances do not contain gold-reactive thiol group, they react with laser-synthesized gold nanoparticles, yielding to a drastic reduction of the nanoparticle size. Figure 7b illustrates the effect of the reduction of nanoparticle mean size under the use of a biopolymer polyethylene glycol (PEG). One can see that the nanoparticles' mean size and size dispersion can be reduced down to 3 nm with the size dispersion not exceeding 1.5 nm FWHM. We believe that such reduction of nanoparticle size is a result of the hydrogen bonding of the –OH groups of these compounds and the $-O^-$ at the gold surface. The molecules of PEG cover gold nanoclusters just after ablation and act like "bumpers", limiting contact between particles, preventing their coalescence (when the particles are still "hot") and aggregation (when the particles are "cold"). Similar mechanism takes place during laser ablation in aqueous solutions of other polymers (dextran etc.) [72] and oligosaccharides (cyclodextrin) [30]. Thus, OH groups of different biocompatible compounds can efficiently react with oxidized gold surface leading to the reduction of the nanoparticle size. It is important that in contrast to SDS or other surfactants previously used to control the nanoparticle size [27], biopolymers and oligosaccharides are essentially biocompatible. Moreover, the ultra-pure laser-ablated nanoparticles can be functionalized by a proper chemical modification of chemicals. We believe that this gives a huge advantage over the chemically produced nanoparticles for nano-engineering and functionalization of nanoparticles produced, as well as for a solution of toxicity problems. In particular, PEG is known as one of best materials to avoid the immune response in "in vivo" applications of inorganic nanoparticles. When covered by PEG, the nanoparticles become invisible for the immune system. In the case of laser-synthesized nanoparticles, one does not need to use any intermediate chemical group to link nanoparticles to PEG, as it takes place in the case of chemically synthesized nanoparticles.

Conclusions

We reviewed on the development, in our Institute, of various laser-assisted methodologies for nanofabrication in the gaseous and liquid environment. The methodologies imply the fabrication of nanoparticles/nanostructures either within the laser irradiation spot on the target surface or in the ablated species. Laser-synthesized nanomaterials exhibit unique optical properties and are exempt of toxicity, which make them very important for photovoltaics, optoelectronics, biological sensing, imaging and therapeutics.

Acknowledgments The authors are grateful to Agence Nationale de Recherche (ANR) and Ion Beam Services (IBS company) for Plasma Immersion doping of the black silicon.

References

1. L.T. Canham, Appl. Phys. Lett. **57**, 1046 (1990)
2. A.G. Cullis, L.T. Canham, P.D. Calcott, J. Appl. Phys. **82**, 909 (1997)
3. D. Kovalev, E. Gross, N. Künzner, F. Koch, V.Y. Timoshenko, M. Fujii, Phys. Rev. Lett. **8913**, 137401 (2002)
4. V.Y. Timoshenko, A.A. Kudryavtsev, L.A. Osminkina, A.S. Vorontsov, Y.V. Ryabchikov, I.A. Belogorkhov, D. Kovalev, P.K. Kashkarov, JETP Lett. **83**, 423 (2006)
5. M. Kerker, *The Scattering of Light and Other Electromagnetic Radiation* (Academic Press, New York, 1969)
6. U. Kreibig, M. Vollmer, *Optical Properties of Metal Clusters* (Springer, Berlin, 1996)
7. S. Nie, S.R. Emory, Science **275**, 1102–1106 (1997)
8. K. Li, X. Li, M. Stockman, D. Bergman, Phys. Rev. B **71**, 115409 (2005)
9. J. Yao, Z. Liu, Y. Liu, Y. Wang, C. Sun, G. Bartal, A. Stacy, X. Zhang, Science **321**, 930 (2008)
10. A.N. Grigorenko, N.W. Roberts, M.R. Dickinson, Y. Zhang, Nat. Photon. **2**, 365–368 (2008)
11. A.V. Kabashin, M. Meunier, Recent advances, in *Laser Processing Material*, ed. by J. Perriere, E. Millon, E. Fogarassi (Elsevier, Amsterdam, 2006), pp. 1–36
12. A.M. Prokhorov, V.I. Konov, I. Ursu, I.N. Mikhailescu, *Laser Heating of Metals* (Hilger, Bristol, 1990)
13. D.J. Krajnovich, J.E. Vazquez, J. Appl. Phys. **73**, 3001 (1993)
14. T.-H. Her, R.J. Finlay, C. Wu, S. Deliwala, E. Mazur, Appl. Phys. Lett. **73**, 1673 (1998)
15. A.J. Pedraza, J.D. Fowlkes, D.H. Lowndes, Appl. Phys. Lett. **74**, 2322 (1999)
16. F. Costache, M. Henyk, J. Reif, Appl. Surf. Sci. **186**, 352 (2002)
17. I.A. Movtchan, W. Marine, R.W. Dreyfus, H.C. Le, M. Sentis, M. Autric, Appl. Surf. Sci. **96–98**, 251 (1996)
18. D.B. Geohegan, A.A. Puretzky, G. Duscher, S.J. Pennycook, Appl. Phys. Lett. **73**, 438 (1998)
19. D.B. Geohegan, A.A. Puretzky, G. Duscher, S.J. Pennycook, Appl. Phys. Lett. **72**, 2987 (1998)
20. M.E. Povarnitsyn, T.E. Itina, M. Sentis, K.V. Khishenko, P.R. Levashov, Phys. Rev. B Phys. B **75**, 235414 (2007)
21. E. Werwa, A.A. Seraphin, L.A. Chiu, C. Zhou, K.D. Kolenbrander, Appl. Phys. Lett. **64**, 1821 (1994)
22. Y. Yamada, T. Orii, I. Umezu, Sh. Takeyama, T. Yoshida, Jpn. J. Appl. Phys. **35**, 1361 (1996)
23. A.V. Kabashin, J.-P. Sylvestre, S. Patskovsky, M. Meunier, J. Appl. Phys. **91**, 3248 (2002)
24. A. Pereira, A. Cros, Ph. Delaporte, S. Georgiou, A. Manousaki, W. Marine, M. Sentis, Appl. Phys. A **79**, 1433 (2004)

25. A.J. Henglein, Phys. Chem. **97**, 5457 (1993)
26. J. Nedderson, G. Chumanov, T.M. Cotton, Appl. Spectrosc. **47**, 1959 (1993)
27. F. Mafuné, J.-Y. Kohno, Y. Takeda, T. Kondow, H. Sawabe, J. Phys. Chem. B **104**, 8333 (2000)
28. A.V. Kabashin, M. Meunier, J. Appl. Phys. **94**, 7941 (2003)
29. J.-P. Sylvestre, A.V. Kabashin, E. Sacher, M. Meunier, Appl. Phys. A **80**, 753 (2004)
30. A.V. Kabashin, M. Meunier, C. Kingston, J.H.T. Luong, J. Phys. Chem. B **107**, 4527 (2003)
31. J.-P. Sylvestre, A.V. Kabashin, E. Sacher, M. Meunier, J.H.T. Luong, J. Am. Chem. Soc. (Commun.) **126**, 7176 (2004)
32. A.V. Kabashin, M. Meunier, J. Photochem. Photobiol. A **182**, 330–334 (2006)
33. S. Besner, A.V. Kabashin, F.W. Winnik, M. Meunier, Appl. Phys. A **93**, 955–959 (2008)
34. V. Tokarev, W. Marine, M. Sentis, C. Prat, J. Appl. Phys. **77**, 4714 (1995)
35. B.N. Chichkov, C. Momma, S. Nolte, F. Von Alvensleben, A. Tünnermann, Appl. Phys. A **63**, 109 (1996)
36. J.D. Parisse, W. Marine, M. Sentis, J. Phys. IV **9**(5), PR5–149 (1999)
37. C. Wu, C.H. Crouch, L. Zhao, E. Mazur, Appl. Phys. Lett. **81**, 1999 (2002)
38. J. Reif, F. Costache, M. Henyk, S.V. Pandelov, Appl. Surf. Sci. **197–198**, 891 (2002)
39. G. Daminelli, J. Krüger, W. Kautek, Thin Solid Films **467**, 334 (2004)
40. S. Besner, J.-Y. Degorce, A.V. Kabashin, M. Meunier, Appl. Surf. Sci. **247**, 163–168 (2005)
41. A.Y. Vorobyev, C. Guo, Appl. Phys. Lett. **92**, 041914 (2008)
42. M. Halbwax, T. Sarnet, Ph. Delaporte, M. Sentis, H. Etienne, F. Torregrosa, V. Vervisch, I. Perichaud, S. Martinuzzi, Thin Solid Films **516**, 6791 (2008)
43. A. Pereira, Ph. Delaporte, M. Sentis, A. Cros, W. Marine, A. Basillais, A.L. Thomann, C. Leborgne, N. Semmar, P. Andreazza, T. Sauvage, Thin Solid Films **453–454**, 16 (2004)
44. A.V. Kabashin, M. Meunier, Appl. Phys. Lett. **82**, 1619 (2003)
45. D. Yang, A. Kabashin, V.-G. Pilon-Marien, E. Sacher, M. Meunier, J. Appl. Phys. **95**, 5722 (2004)
46. A.V. Kabashin, M. Meunier, Mat Sci. Eng. B **101**, 60–64 (2003)
47. A.V. Kabashin, F. Magny, M. Meunier, J. Appl. Phys. **101**, 054311 (2007)
48. A.V. Kabashin, A. Trudeau, W. Marine, M. Meunier, Appl. Phys. Lett. **91**, 201101 (2007)
49. A.V. Kabashin, A. Trudeau, W. Marine, M. Meunier, Appl. Phys. A **91**, 621 (2008)
50. F.V. Bunkin, V.I. Konov, A.M. Prokhorov, V.B. Fedorov, JTP Lett. **9**, 371 (1969)
51. T. Itina, J. Hermann, Ph. Delaporte, M. Sentis, Appl. Surf. Sci. **128**, 27 (2003)
52. Y.P. Raizer, *Laser-induced Discharge Phenomena* (Consultants Bureau, New York, 1977)
53. M.G. Drouet, H. Pepin, Appl. Phys. Lett. **28**, 426 (1976)
54. V.V. Korobkin, R.V. Serov, Pisma Zh. Eksp. Teor. Fiz. **4**, 103 (1966). [see also J. Exp. Theor. Phys. Lett. **4**, 70 (1966)]
55. A.V. Kabashin, P.I. Nikitin, Quantum Electron. **27**, 536 (1997)
56. A.V. Kabashin, P.I. Nikitin, W. Marine, M. Sentis, Appl. Phys. Lett. **73**, 25 (1998)
57. A. Pereira, D. Grojo, M. Chaker, Ph. Delaporte, D. Guay, M. Sentis, Small **4**, 572 (2008)
58. K. Piglmayer, R. Denk, D. Bauerle, Appl. Phys. Lett. **80**, 4693–4695 (2002)
59. S.M. Huang, M.H. Hong, B.S. Luk'yanchuk, Y.W. Zheng, W.D. Song, Y.F. Lu, T.C. Chong, J. Appl. Phys. **92**, 2495–2500 (2002)
60. S.M. Huang, Z. Sun, B.S. Luk'yanchuk, M.H. Hong, L.P. Shi, Appl. Phys. Lett. **86**, 161911 (2005)
61. Y. Lu, S.C. Chen, Nanotechnology **14**, 505–508 (2003)
62. J.N. Anker, W.P. Hall, O. Lyandres, N.C. Shah, J. Zhao, R.P. Van Duyne, Nature Mater. **7**, 442–453 (2008)
63. A.V. Kabashin, P. Evans, S. Patskovsky, G. Wurtz, W. Hendren, W. Dickson, R.J. Pollard, V. Podolsky, A.V. Zayats, Nature Mater. **8**, 867–871 (2009)
64. F.F. Abraham, *Homogeneous Nucleation Theory: The Pretransition Theory of Vapor Condensation* (Academic Press, New York, 1974)
65. D. Kashchiev, *Nucleation: Basic Theory with Applications* (Butterworth-Heinemann, Oxford, 2000)
66. A.V. Kabashin, M. Charbonneau-Lefort, M. Meunier, R. Leonelli, Appl. Surf. Sci. **168**, 328 (2000)
67. A.V. Kabashin, M. Meunier, R. Leonelli, J. Vacuum Sci. Tech. B **19**, 2217 (2001)
68. S.M. Prokes, Appl. Phys. Lett. **62**, 3244 (1993)
69. Y. Kanemitsu, T. Ogawa, K. Shiraishi, K. Takeda, Phys. Rev. B **48**, 4883 (1993)
70. A. Vogel, J. Noack, K. Nahen, D. Theisen, S. Busch, U. Parlitz, D.X. Hammer, G.D. Noojin, B.A. Rockwell, R. Birngruber, Appl. Phys. B **68**, 271 (1999)
71. J.-P. Sylvestre, S. Poulin, A.V. Kabashin, E. Sacher, M. Meunier, J.H.T. Luong, J Phys Chem B **108**, 16864–16869 (2004)
72. S. Besner, A.V. Kabashin, M. Meunier, F.M. Winnik, J Phys. Chem C. **113**, 9526–9531 (2009)
73. D. Rioux, M. Laferriere, A. Douplik, D. Shah, L. Lilge, A.V. Kabashin, M. Meunier, J. Biomed. Optics **14**, 021010 (2009)